SRI International

ON THE IMAGING OF FRACTAL SURFACES

Technical Note No. 390

December 16, 1986

By: Alex Pentland

Artificial Intelligence Center
Computer Science and Technology Division

and

Paul Kube

Computer Science Division
University of California at Berkeley

333 Ravenswood Ave. • Menlo Park, CA 94025
(415) 326-6200 • TWX: 910-373-2046 • Telex: 334-486

December 16, 1986

On The Imaging of Fractal Surfaces

Paul Kube and Alex Pentland

Computer Science Division
University of California, Berkeley
and
Artificial Intelligence Center, SRI International
Menlo Park, California

ABSTRACT [1]

We examine the imaging of standard Brownian Fractal surfaces, and find that, given certain assumptions, a Fractal surface with power spectrum proportional to $f^{-\beta}$ has an image with power spectrum proportional to $f^{2-\beta}$.

1 Introduction

Fractal Brownian functions have found widespread use in computer graphics because they produce surfaces that closely resemble natural surfaces. It is natural, therefore, to ask if we may apply such an attractive model of natural surface shape to the problems of image analysis. Pentland [1] showed, by modeling natural surfaces using Brownian Fractals, that interesting information about the imaged surface could be obtained.

In his analysis Pentland modeled the imaged surface using a vector-valued plane-to-surface-normal Brownian Fractal function. The non-constructive nature of this model, however, places unfortunate restrictions upon its usefulness. In this paper we analyze the imaging of surfaces modelled by Fractal Brownian plane-to-elevation functions of the sort standardly used in computer graphics. We thus obtain a model of surface and image that is

[1] This research was made possible by National Science Foundation, Grant No. DCR-85-19283, by Defense Advanced Research Projects Agency contract no. MDA 903-83-C-0027, and by grants from the Systems Development Foundation and the Alfred P. Sloan Foundation. We would like to thank Gene Switkes and Eugene Wong of Berkeley and Andy Hanson of SRI for helpful discussions.

constructive in nature, and therefore of potentially greater use in image analysis.

2 Standard Fractal Brownian Models

In one topological dimension, a Fractal Brownian line function $V_H(t)$ has zero-mean Gaussian increments with variance

$$< [V_H(t+\delta) - V_H(t)]^2 > \quad \propto \quad |\delta|^{2H} \tag{1}$$

where $H \epsilon (0,1)$. H is related to the *fractal dimension* D of $V_H(t)$ by

$$D = 2 - H \tag{2}$$

Further, $V_H(t)$ has a random-phase Fourier spectrum with power $\mathbf{F}_H(f)$ such that

$$\mathbf{F}_H(f) \quad \propto \quad f^{-\beta} \tag{3}$$

H is related to β by

$$\beta = 2H + 1 \tag{4}$$

In two topological dimensions, any "slice" through an isotropic Fractal Brownian surface $V_H(x,y)$ is a Fractal Brownian line function of identical H. Thus we want

$$< [V_H(x + \delta\cos\gamma, y + \delta\sin\gamma) - V_H(x,y)]^2 > \quad \propto \quad |\delta|^{2H} \tag{5}$$

independent of γ. Voss [2] shows that this requires the two-dimensional power spectrum $\mathbf{F}_H(f,\theta)$ of the surface to be

$$\mathbf{F}_H(f,\theta) \quad \propto \quad f^{-\beta} \tag{6}$$

where

$$\beta = 2H + 2 \tag{7}$$

These two-dimensional surfaces can be constructed by filtering Gaussian noise [2], or (more efficiently and flexibly) by constructing the an appropriate Laplacian Pyramid [3]. Those in computer graphics often use a recursive subdivision algorithm to approximate true Fractal Brownian surfaces [4].

3 Imaging of Fractal Brownian Surfaces

Let $z = V_H(x, y)$ be a Fractal Brownian surface, and let us assume that:

(1) the surface is Lambertian (we will later partially relax this assumption),

(2) the surface is illuminated by (possibly several) distant point sources,

(3) the surface is not self-shadowing.

We will also take $z < 0$ within the region of interest, and assume orthographic projection onto the x, y plane.

We will let $\mathbf{L} = (\cos\tau \sin\sigma, \sin\tau \sin\sigma, \cos\sigma)$ be the unit vector in the mean illuminant direction, where τ is the *tilt* of the illuminant (the angle the image plane component of the illuminant vector makes with the x-axis) and σ is its *slant* (the angle the illuminant vector makes with the z-axis).

Then the normalized image intensity $I(x, y)$ will be

$$I(x, y) = \frac{p \cos\tau \sin\sigma + q \sin\tau \sin\sigma + \cos\sigma}{(p^2 + q^2 + 1)^{1/2}} \tag{8}$$

where

$$p = \frac{\partial}{\partial x} V_H(x, y) \tag{9}$$

$$q = \frac{\partial}{\partial y} V_H(x, y) \tag{10}$$

[Note: as true Fractal Brownian surfaces are, strictly, nowhere differentiable, we will assume throughout an approximation smoothed sufficiently to allow p and q to exist. See [5] for justification of this approach.]

3.1 Spectral Properties

If we then take the Taylor series expansion of $I(x, y)$ about $p, q = 0$ through the quadratic terms, we obtain

$$I(x, y) \approx \cos\sigma + p \cos\tau \sin\sigma + q \sin\tau \sin\sigma - \frac{\cos\sigma}{2}(p^2 + q^2) \tag{11}$$

This expression gives an excellent approximation if $p, q \ll 1$. We note that for real surfaces, such as mountains, the maximum surface slope rarely is more than 15°, i.e., typically $p^2 + q^2 < 0.1$. Under these conditions the linear terms of Eqn. (11) will dominate the power spectrum except when

the average illuminant is within $\pm 6°$ of the viewer's position, i.e., when $\sin\sigma < 0.1$.

The complex Fourier spectrum $F_H(f,\theta)$ of $V_H(x,y)$ is, from Eqn. (6),

$$F_H(f,\theta) = f^{-\beta/2} e^{i\phi_{f,\theta}} \tag{12}$$

where ϕ is a random variable uniformly distributed on $(0, 2\pi)$, and $\phi_{f,\theta}$ is the value "drawn" at position (f,θ) in the Fourier plane.

Now since p and q are partial derivatives of V_H, their transforms F_p and F_q are related to F_H in an elementary fashion. We can write

$$F_p(f,\theta) = 2\pi \cos\theta f^{1-\beta/2} e^{i(\phi_{f,\theta}+\pi/2)} \tag{13}$$

$$F_q(f,\theta) = 2\pi \sin\theta f^{1-\beta/2} e^{i(\phi_{f,\theta}+\pi/2)} \tag{14}$$

3.1.1 Case 1

When p, q are small and the illuminant is not behind the viewer (e.g., $\sin\sigma > 0.1$) then we may neglect the quadratic terms of Eqn. (11) and consider

$$I_1(x,y) = \cos\sigma + p\cos\tau\sin\sigma + q\sin\tau\sin\sigma \tag{15}$$

In this case, the Fourier transform of the image I_1 is (ignoring the DC term):

$$F_{I_1}(f,\theta) = 2\pi \sin\sigma f^{1-\beta/2} e^{i(\phi_{f,\theta}+\pi/2)} [\cos\theta\cos\tau + \sin\theta\sin\tau] \tag{16}$$

and the power spectrum is

$$\mathbf{F}_{I_1}(f,\theta) = 4\pi^2 \sin^2\sigma f^{2-\beta} [\cos\theta\cos\tau + \sin\theta\sin\tau]^2 \tag{17}$$

This spectrum depends, as expected, upon the illuminant direction. As with the Fractal surface itself, however, the spectral falloff is isotropic: the log of the power spectrum of the image has slope $2-\beta$ with respect to log frequency at almost all orientations (excepting a set of measure zero where $\theta = \tau \pm \pi/2$).

3.2 Case 2

When the mean illuminant vector is almost parallel to the viewing direction (i.e., $\sin\sigma \approx 0$) the quadratic terms of Eqn. (11) can dominate and the image of a fractional Brownian surface will look like

$$I_2(x,y) = \cos\sigma(1 - (p^2+q^2)/2) \tag{18}$$

To within a constant factor, and ignoring DC, the power spectrum $\mathbf{F}_{I_2}$ of this image will be the Fourier transform of the autocorrelation function $R_{p^2+q^2}$ of p^2+q^2, which we now investigate. The autocorrelation function is written

$$\begin{aligned} R_{p^2+q^2}(x,y) &= < [p(x^*,y^*)^2 + q(x^*,y^*)^2] \\ &\qquad [p(x^*+x,y^*+y)^2 + q(x^*+x,y^*+y)^2] > \\ &\quad - < p(x^*,y^*)^2 + q(x^*,y^*)^2 > \\ &\qquad < p(x^*+x,y^*+y)^2 + q(x^*+x,y^*+y)^2 > \end{aligned} \tag{19}$$

where <> denotes expectation. Since p and q are stationary, we can write

$$\begin{aligned} R_{p^2+q^2}(x,y) &= < p_{00}^2 p_{xy}^2 > + < q_{00}^2 q_{xy}^2 > \\ &+ < q_{00}^2 p_{xy}^2 > + < p_{00}^2 q_{xy}^2 > \\ &- < p_{00}^2 >< p_{xy}^2 > - < q_{00}^2 >< q_{xy}^2 > \\ &- < q_{00}^2 >< p_{xy}^2 > - < p_{00}^2 >< q_{xy}^2 > \end{aligned} \tag{20}$$

where we have put p_{xy} for $p(x,y)$, etc. Since p and q are Gaussian processes, the first four terms on the right hand side of Eqn. (20) can be rewritten

$$< p_{00}^2 p_{xy}^2 > = 2 < p_{00} p_{xy} >^2 + < p_{00}^2 >< p_{xy}^2 > \tag{21}$$

$$< q_{00}^2 q_{xy}^2 > = 2 < q_{00} q_{xy} >^2 + < q_{00}^2 >< q_{xy}^2 > \tag{22}$$

$$< q_{00}^2 p_{xy}^2 > = 2 < q_{00} p_{xy} >^2 + < q_{00}^2 >< p_{xy}^2 > \tag{23}$$

$$< p_{00}^2 q_{xy}^2 > = 2 < p_{00} q_{xy} >^2 + < p_{00}^2 >< q_{xy}^2 > \tag{24}$$

Thus

$$\begin{aligned} R_{p^2+q^2}(x,y) &= 2(< p_{00} p_{xy} >^2 + < p_{00} q_{xy} >^2 \\ &\qquad + < q_{00} p_{xy} >^2 + < q_{00} q_{xy} >^2) \end{aligned} \tag{25}$$

We know what the Fourier transforms of the autocorrelations of p and of q are; they are just the power spectra of p and of q respectively, easily obtained from Eqns. (13) and (14):

$$\mathbf{F}_p(f,\theta) = 4\pi^2 \cos^2\theta f^{2-\beta} \tag{26}$$

$$\mathbf{F}_q(f,\theta) = 4\pi^2 \sin^2\theta f^{2-\beta} \tag{27}$$

To see what the Fourier transform of $< p_{00} q_{xy} >=< q_{00} p_{xy} >$ must be, we construct the expression for the autocorrelation R_{I_1} of $I_1(x,y) =$

$(p\cos\tau\sin\sigma + q\sin\tau\sin\sigma)$ and expand it to obtain:

$$\begin{aligned} R_{I_1}(x,y) &= \cos^2\tau\sin^2\sigma < p_{00}p_{xy} > \\ &\quad + \sin^2\tau\sin^2\sigma < q_{00}q_{xy} > \\ &\quad + 2\cos\tau\sin\tau\sin^2\sigma < p_{00}q_{xy} > \end{aligned} \tag{28}$$

If we now take the Fourier transform of this expression we find, as we already know the power spectrum of I_1 (cf. Eqn. (17)), and the power spectra of p and q, that we can solve for the Fourier transform F_{pq} of $< p_{00}q_{xy} >$. We obtain

$$F_{pq} = 4\pi^2\sin\theta\cos\theta f^{2-\beta} \tag{29}$$

With this result, we find that the Fourier transform of $R_{p^2+q^2}(x,y)$ is then

$$F_R = 2(\mathbf{F}_p * \mathbf{F}_p) + 4(F_{pq} * F_{pq}) + 2(\mathbf{F}_q * \mathbf{F}_q) \tag{30}$$

where $*$ denotes convolution. In Cartesian coordinates, we can write

$$F_R(u,v) = 2\int_{-\infty}^{\infty}\int_{-\infty}^{\infty} \frac{[u^*(u^*-u)+v^*(v^*-v)]^2}{[(u^{*2}+v^{*2})((u^*-u)^2+(v^*-v)^2)]^{\beta/2}} du^* dv^* \tag{31}$$

This integral diverges at $u = v = 0$ for any β. When $\beta < 3$, it diverges at all u, v because of behavior of the integrand as $u^*, v^* \to \infty$. We note, though, that the spectral power of a real surface does not go to infinity as frequency goes to zero, and any sufficiently high frequency components of a surface can be ignored in a model of a physically realizable imaging process; thus F_R can be taken as well defined everywhere.

To find an approximation to F_R, note that since $\beta > 2$, $f^{2-\beta}$ becomes quickly very large as f approaches 0. Therefore we might think of the self-convolutions represented in Eqn. (30) as instead being convolutions with a localized averaging kernel, say a Gaussian with small variance. Then (at least for frequencies sufficiently far from zero)

$$\mathbf{F}_p * \mathbf{F}_p \approx \mathbf{F}_p \qquad F_{pq} * F_{pq} \approx F_{pq} \qquad \mathbf{F}_q * \mathbf{F}_q \approx \mathbf{F}_q \tag{32}$$

and thus

$$\log \mathbf{F}_{I_2} \quad \propto \quad \log F_R \quad \propto \quad 2-\beta \tag{33}$$

The conclusion, therefore, is that when the mean illumination is at the viewer's position the image will have a power spectrum falloff approximately proportional to $f^{2-\beta}$, i.e., the same relationship between surface Fractal

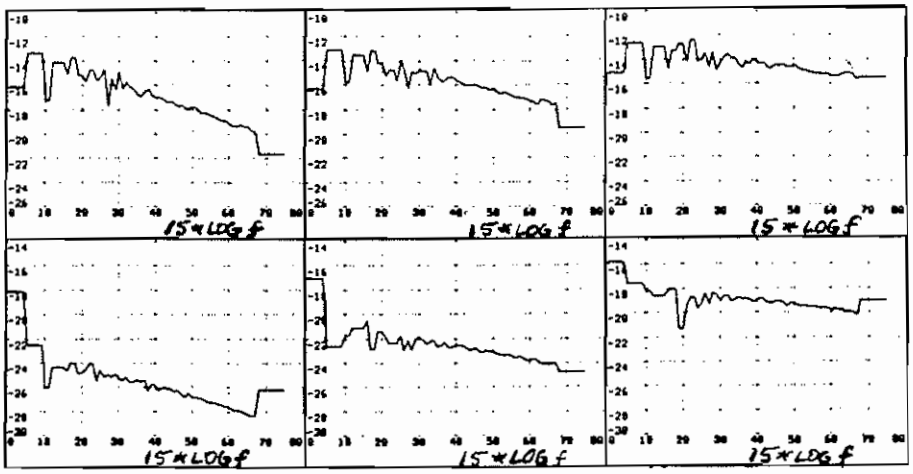

Figure 1: *Comparison of predicted (top row) versus the actual (bottom row) radially-averaged log Fourier power versus log frequency for images of Fractal dimension* $D = 2.25, 2.5, 2.75$, *assuming the illuminant is at the viewer's position.*

scaling parameter and image Fractal scaling parameter that we found with oblique illumination. This conclusion is supported by the results of the following simulation.

3.2.1 Simulation

Range maps $z = V_H(x, y)$ for $H = 0.25$, 0.5 and 0.75 (corresponding to surface of Fractal dimension of $D = 2.75$, 2.5, and 2.25) were illuminated and viewed along the z axis and the power spectrum exponent was observed for the resulting image. For each H, V_H was scaled to have $E(|p|) = 0.1$. Figure 1 shows graphs of the log Fourier power versus log frequency of the images' spectrum; power at a frequency was averaged over all orientations at that frequency.

3.3 Oblique Viewpoints

So far we have considered only views straight down on the surface. We would like to consider the case of oblique views of the surface. Without loss of generality we may consider only the case where in the viewer's co-ordinate

system (x^*, y^*, z^*) the surface has partials (p^*, q^*) such that

$$p^* = p + c \qquad q^* = q \tag{34}$$

where (p, q) are (as in Eqns. (9) and (10) the partials measured in the *surface's* co-ordinate system. Thus the surface has an average slope $dz^*/dx^* = c$ with regard to the viewer.

In this case Eqn. (11) becomes

$$\begin{aligned} I(x,y) &= [\cos\sigma + (p+c)\cos\tau\sin\sigma + q\sin\tau\sin\sigma](1+c^2)^{-1/2} \\ &\quad -\frac{\cos\sigma + c\cos\tau\sin\sigma}{2}(p^2+q^2) \end{aligned} \tag{35}$$

If continue to assume that p,q are small, then in the *oblique* co-ordinate system the frequency $f^* = \delta f$, where $\delta = (1+c)^{-1}\cos^2\theta + \sin^2\theta$, and f is the freqency in the surface co-ordinate system (i.e., there is foreshortening). Similarly, the orientation θ^* in the oblique co-ordinate system is a function of the orientation θ in the surface co-ordinate system. Thus Eqns. (13) and (14) become:

$$F_{p^*}(f^*, \theta^*) = 2\pi\cos\theta^*(\theta)\delta^{1/2-\beta/4} f^{1-\beta/2} e^{i(\phi_{f,\theta}+\pi/2)} \tag{36}$$

$$F_{q^*}(f^*, \theta^*) = 2\pi\sin\theta^*(\theta)\delta^{1/2-\beta/4} f^{1-\beta/2} e^{i(\phi_{f,\theta}+\pi/2)} \tag{37}$$

If, as in Case 1 above, we are in a condition in which we may ignore the quadratic terms of Eqn. (35), we then find that the complex spectrum of the image (again ignoring the DC terms) is given by:

$$\begin{aligned} F_I(f^*, \theta^*) &= 2\pi(1+c^2)^{-1/2} f^{1-\beta/2} e^{i(\phi_{f,\theta}+\pi/2)} \\ &\qquad [(1-c)\delta^{1/2-\beta/4}\cos\theta^*(\theta)\cos\tau + \sin\theta^*(\theta)\sin\tau] \\ &\quad -\cos\theta^*(\theta)\cos\sigma\pi\delta^{1/2-\beta/4} f^{1-\beta/2} e^{i(\phi_{f,\theta}+\pi/2)} \end{aligned} \tag{38}$$

and thus the power spectrum of the image, although now complexly dependant upon the illuminant direction and average angle of view, still has an isotropic falloff proportional to $f^{2-\beta}$ as in the non-oblique case. A similar result holds for the case in which the quadratic terms of Eqn. (35) dominate.

3.4 Non-isotropic Surfaces

We have considered only Fractal surfaces with uniform spatial statistics; however many natural surfaces (e.g., tree bark) can be modeled only with anisotropic statistics. We would therefore like to consider surfaces $V_H(x, y)$ with "stretched" spectra:

$$F(f, \theta) = \delta f^{-\beta/2} e^{i\phi_{f,\theta}} \tag{39}$$

where again $\delta = (1 + c)^{-1} \cos^\theta + \sin^2 \theta$. Examining Eqns. (6) - (33) using this new surface function, we find that this new multiplicative stretching factor simply propagates through our calculations, resulting in an "stretched" image spectrum whose spectral falloff, however, is still isotropic and whose rate is the same as in the isotropic case.

3.5 Occlusion, Shadows and Highlights

We can, to a limited extent, analyze cases involving non-Lambertian surfaces, self-shadowing and cast shadows. The following sections are our first step towards a more complete analysis.

3.5.1 Occlusions and Shadows

When the viewing angle becomes sufficiently oblique the high points of the surface will begin to occlude the remainder of the surface; for viewing angles that are extremely oblique, the effects of such occlusion will begin to dominate the image. Similarly, when the illuminant becomes sufficiently oblique, there will be self-shadowed, and when the illuminant direction becomes nearly tangential to the surface then the image will be dominated by the effects of cast shadows.

When a surface occludes itself, there is a discontinuous jump between points that are adjacent in the image. Because of this jump, the orientation at these image-adjacent points will be only very weakly correlated thus producing a step discontinuity in the image. The spectrum of such a discontinuity is proportinal to $1/f$; i.e., the spectrum of a step discontinuity falls off much more slowly than does the normal image spectrum. As a result when such steps are added to the image the high freqency content of the image quickly becomes dominated by their spectral contribution.

Similarly, casts shadows introduce large amplitude step edges into the image. Again, the high frequency content of such edges quickly comes to dominate the spectral content of the image.

3.5.2 Highlights

Highlights occur when the surface orientation exactly reflects the incident illumination toward the viewer; i.e., they are associated with a particular *level-sets* of the (independent) p and q functions. That is, hightlights occur at the intersection of separate level-sets of the p and q functions. From Mandelbrot [6], we know that both the level-set of a Fractal Brownian surface and the surface itself have the same scaling parameter H. Thus the set of image highlights will be the intersection of two sets of dimension $D = 2H+1$. We speculate that the dimension of this intersection set is $D = 2H$. If so, then by identifing the set of surface hightlights we can (by estimating their Fractal scaling parameter) directly obtain the Fractal scaling parameter of the surface itself.

4 Summary

We have analyzed the imaging of Fractal Brownian surfaces such as are constructed in computer graphics. We have found that, given the Lambertian assumption and no self-shadowing, that the image of a Fractal Brownian surface with spectrum proportional to $f^{-\beta}$ has a spectrum proportional to $f^{2-\beta}$. Thus the main result of this paper is that, in the case of the non-isotropic Brownian Fractals used in computer graphics, we can use the Fractal scaling parameter (spectral falloff) of the image to predict the Fractal scaling parameter of the surface. We also have shown that this result is not affected by multiplicative "stretching" of the surface and, given that $p^2 + q^2$ is small, is relatively unaffected by viewing position.

These results agree with those obtained using an isotropic Fractal surface model [1]. The major advance of this paper is that, because we have used a Fractal surface model that is defined constructively, we can now easily synthesize surfaces whose images have the desired Fractal scaling behavior.

And finally, it appears that self-shadowing and self-occlusion produce image features which "swamp" the normal Fractal scaling characteristics with f^{-1} noise. The fractal scaling parameter of imaged highlights, however, appears provide us with a method of obtaining an independent estimate of the surface's Fractal scaling parameter.

5 REFERENCES

[1] Pentland, A. P. (1984) Fractal-Based Description of Natural Scenes, *IEEE Trans. on Pattern Analysis and Mach. Intel.*, Vol. 6, No. 6, 661-674.

[2] Voss, R. F. (1985) Random Fractal Forgeries, in *Fundamental Algorithms for Computer Graphics*, R.A. Earnshaw (Ed.), Springer-Verlag, Berlin.

[3] Pentland, A. P. (1986) On Describing Complex Surfaces, *Image and Vision Computing*, Vol 3, No. 4, 153-162.

[4] Fournier, A., Fussel, D., and Carpenter, L. (1982). Computer rendering of stochastic models, *Comm. ACM*, Vol. 25, No. 6, 371-384.

[5] Mandelbrot, B. B. and Van Ness, J. W., (1968). Fractional Brownian motions, fractional noises and applications, *SIAM Review*, Vol. 10, No. 4, 422-437.

[6] Mandelbrot, B. B., (1982) The fractal Geometry of nature, Freeman, San Francisco.